FEBS Letters

FEBS PRESS science publishing by scientists

Structural and biochemical analysis of a phosin from *Streptomyces chartreusis* reveals a combined polyphosphate- and metal-binding fold

Sebastiaan Werten[1], Nils Hinnerk Rustmeier[2], Maximilian Gemmer[2], Marie-Joëlle Virolle[3] and Winfried Hinrichs[2]

1 Division of Biological Chemistry, Biocenter, Medical University of Innsbruck, Austria
2 Department of Molecular Structural Biology, Institute for Biochemistry, University of Greifswald, Germany
3 Institute for Integrative Biology of the Cell (I2BC), CEA, CNRS, Univ. Paris-Sud, Université Paris-Saclay, France

Correspondence
S. Werten, Division of Biological Chemistry, Biocenter, Medical University of Innsbruck, Innrain 80, 6020 Innsbruck, Austria
Tel: +43 512 9003 70336
E-mail: sebastiaan.werten@i-med.ac.at

(Received 12 May 2019, revised 4 June 2019, accepted 5 June 2019, available online 17 June 2019)

doi:10.1002/1873-3468.13476

Edited by Stuart Ferguson

X-ray crystallographic analysis of a phosin (PptA) from *Steptomyces chartreusis* reveals a metal-associated, lozenge-shaped fold featuring a 5–10 Å wide, positively charged tunnel that traverses the protein core. Two distinct metal-binding sites were identified in which the predominant metal ion was Cu^{2+}. In solution, PptA forms stable homodimers that bind with nanomolar affinity to polyphosphate, a stress-related biopolymer acting as a phosphate and energy reserve in conditions of nutrient depletion. A single protein dimer interacts with 14–15 consecutive phosphate moieties within the polymer. Our observations suggest that PptA plays a role in polyphosphate metabolism, mobilisation or sensing, possibly by acting in concert with polyphosphate kinase (Ppk). Like Ppk, phosins may influence antibiotic synthesis by streptomycetes.

Keywords: antibiotics; conserved histidine α-helical domain; nutritional stress; phosphate metabolism; secondary metabolism; signalling

Streptomyces are Gram-positive, filamentous soil bacteria, capable of producing a large variety of secondary metabolites. Many of these bioactive molecules, which enable the genus to thrive in highly competitive natural environments, are used as therapeutics or phytosanitary agents in medicine and agriculture [1,2]. Although *Streptomyces* have been amongst the most prolific sources of clinically relevant antibiotics for decades [3], a recent estimate suggests that only 10% of the metabolic diversity of the genus has been explored, with the vast majority of biosynthetic pathways remaining silenced under typical laboratory conditions [4–6]. To unlock the full chemical repertoire of *Streptomyces* and reveal new molecules of biomedical interest, a better understanding is needed of the intricate regulatory network that governs secondary metabolism.

Interestingly, the most efficient trigger of antibiotic biosynthesis in *Streptomyces* appears to be a nutritional limitation in inorganic phosphate (P_i), which correlates with reduced ATP levels and, consequently, energetic stress [7–9]. As in other bacteria, growth under P_i-limiting conditions leads to the induction of the Pho regulon, governed by the two-component regulatory system PhoR/PhoP [10,11]. As soon as falling P_i concentrations render uptake *via* low-affinity transport systems inadequate, the sensory kinase PhoR autophosphorylates and transfers its phosphoryl group to the response regulator PhoP [12,13]. This transcription factor represses a range of metabolic pathways [10,14,15] while activating the expression of proteins involved in re-establishing P_i homeostasis [16] and the scavenging of P_i from external sources. The latter include secreted phosphatases [10,17,18] as well as

Abbreviations
CHAD, conserved histidine α-helical domain; polyP, polyphosphate.

low- and high-affinity phosphate transport systems, PitH2 and PstSCAB [19,20].

In the model strain *Streptomyces lividans*, one of the genes strongly upregulated in conditions of P_i limitation [21] and found to exert a major negative influence on antibiotic production [22–24] is *ppk*. This gene encodes a polyphosphate (polyP) kinase (Ppk), which uses ATP to synthesise polyP [22]. Under conditions of low ATP content, Ppk mainly acts as an adenosyl diphosphate kinase to catalyse the reverse reaction and regenerate ATP from ADP and polyP [22,23]. As a consequence, the enzyme plays an important role in maintaining energetic homeostasis during phosphate limitation [23].

Interestingly, the gene located immediately downstream of *ppk* encodes a protein comprised of a so-called CHAD (conserved histidine α-helical domain). Although the exact function of CHADs is unclear, these domains frequently occur in conjunction with CYTH (CyaB and thiamine triphosphatase homology) domains and are thought to participate in phosphate and nucleotide metabolism [25]. Based on their unusually high histidine content, CHADs have also been predicted to bind divalent metal ions [25]. More recently, CHAD-containing proteins were found to co-localise with polyP granules in bacteria [26]. They were therefore redesignated 'phosins' or polyP-targeting proteins (PptA or PptB, depending on the presence of additional domains). In the present study, we have structurally and biochemically characterised PptA from a streptomycete, as we hypothesised that this protein, like Ppk, might play a key role in the response to P_i-limiting conditions and the regulation of secondary metabolism.

Materials and methods

Recombinant protein expression and purification

A codon-optimised synthetic gene corresponding to the full-length PptA protein (RefSeq WP_010036273.1) was purchased from Eurofins Genomics (Ebersberg, Germany). This gene was subcloned into pET-28wTEV, a derivative of pET-28b (Merck Chemicals and Life Science GmbH, Darmstadt, Germany) encoding a TEV-protease site in place of the original thrombin recognition sequence. The His_6-tagged protein was expressed in *Escherichia coli* (*E. coli*) strain BL21 (DE3). An overnight preculture, grown from a single colony in LB medium supplemented with 50 μg/ml kanamycin, was diluted 1:100 in antibiotic-containing medium and incubated shaking at 37 °C until the $OD_{600\ nm}$ reached 0.4. Protein expression was induced by adding IPTG to a final concentration of 1 mM, followed by incubation for a further 4 h. Bacteria were collected by centrifugation for 15 min at 4 °C, 5000 ***g***, resuspended in buffer A (20 mM Tris/HCl pH 7.4, 400 mM NaCl) and lysed by sonication (Bandelin Sonopuls HD 2070, 10 min, 50% bursts, 50% power) on ice. Cell debris was removed by centrifugation for 30 min at 4 °C, 40 000 ***g***. The cleared lysate was then applied to a cobalt column (HisPur Cobalt Resin, Thermo Fisher Scientific GmbH, Dreieich, Germany) equilibrated in buffer A. The protein was eluted in buffer A containing 300 mM imidazol. Fractions containing PptA were pooled and incubated for 16 h at room temperature with TEV protease (0.7 mg per 100 mg of PptA), followed by further purification using gel filtration (Superdex 200, GE Healthcare GmbH, Munich, Germany). The resulting protein appeared as a single band on Coomassie-stained SDS/PAGE gels.

X-ray crystallography

Prior to crystallisation, purified PptA was concentrated to 25 mg/ml by means of ultrafiltration (Vivaspin Turbo 15, 10 kDa molecular weight cut-off, Sartorius Stedim Biotech GmbH, Goettingen, Germany). The protein was crystallised using the sitting drop method at 22 °C, using a reservoir solution containing 100 mM MES/HCl pH 6.5 and 1.6 M $MgSO_4$. Before flash-freezing in liquid nitrogen, crystals were incubated for several seconds in five successive buffers containing 100 mM MES/HCl pH 6.5, 1.6 M $MgSO_4$ and increasing amounts (6, 12, 18, 24 or 30%) of glycerol. A bromide derivative was prepared by complementing these buffers with 150, 300, 450, 600 and 750 mM NaBr, respectively.

All crystallographic measurements took place at 100 K. Native and bromide derivative data were recorded on beamline BL14.1 operated by the Joint Berlin MX-Laboratory at the BESSY II electron storage ring (Berlin-Adlershof, Germany) [27]. All data were processed using the program XDS [28]. An overview of data collection statistics can be found in Table 1.

The structure was solved by means of single-wavelength anomalous diffraction (SAD), using Phaser [29] in combination with Phenix [30]. Multiple rounds of manual model building and refinement were carried out using Coot [31,32], Refmac [33,34] and the CCP4 package [35]. Structure refinement statistics have been summarised in Table 1. Figures showing molecular models were prepared using PYMOL 0.99rc6 (DeLano Scientific LLC, Palo Alto, CA, USA). The surface charge distribution of PptA was calculated using ABPS [36] with an ionic strength value of 150 mM.

The structure and X-ray diffraction data for PptA have been deposited in the Protein Data Bank (PDB) with accession number 6RN5.

Metal analysis

X-ray fluorescence analysis [37] of PptA crystals was performed at beamline BL14.1 operated by the Joint Berlin

Table 1. Data collection and refinement statistics for the structure determination of PptA. Values in parentheses pertain to outer resolution shell reflections.

	Native	NaBr
	PDB code 6RN5	
Data collection		
Source	BESSY BL14.1	BESSY BL14.1
Wavelength	0.905002 Å	0.920113 Å
Detector	PILATUS 6M	PILATUS 6M
Space group	$C222_1$	$C222_1$
Cell dimensions		
a	49.3 Å	48.7 Å
b	132.2 Å	132.6 Å
c	116.4 Å	116.0 Å
Resolution range	46.2–2.04 Å (2.16–2.04 Å)	45.8–2.83 Å (3.00–2.83 Å)
R_{sym}	10.6% (91.6%)	10.4% (43.9%)
$<I/\sigma(I)>$	19.2 (2.3)	15.8 (4.3)
Data completeness	98.9% (94.5%)	99.7% (98.4%)
Average redundancy	12.3 (8.9)	6.8 (6.6)
Wilson *B*	38.1 $Å^2$	41.9 $Å^2$
Refinement		
Resolution	46.2–2.04 Å	
Total no. reflections	24,546	
Test set	5% (1228)	
R_{work}	19.1%	
R_{free} (5% test set)	23.7%	
Protein atoms	2155	
Other non-solvent atoms	28	
Solvent atoms	134	
RMSD bond lengths	0.0138 Å	
RMSD bond angles	1.53°	
Average *B*	43.2 $Å^2$	

MX-Laboratory at the BESSY II electron storage ring (Berlin-Adlershof) [27]. Metal concentrations were determined under strongly denaturing conditions (in the presence of 8 M urea) according to the Zincon method described by Säbel *et al.* [38].

Small-angle X-ray scattering

Small-angle X-ray scattering (SAXS) data were recorded at beamline P12 of the EMBL outstation at PETRA III, DESY, Hamburg [39], using a PILATUS 2M pixel detector, a sample-to-detector distance of 3.1 m and a wavelength of 1.24 Å. Measurements covered the momentum transfer range 0.008–0.47 $Å^{-1}$ (defined as $4\pi \sin(\theta)/\lambda$, where 2θ is the scattering angle and λ is the X-ray wavelength). Solutions contained 20 mM Tris/HCl pH 7.4, 400 mM NaCl and 1.3–5.5 mg/ml PptA. The sample temperature was 283 K in all experiments. A capillary flow cell was used to collect 20 successive 50 ms exposures for each sample, revealing no significant change in the course of any one experiment. The data were normalised to the intensity of the transmitted beam and radially averaged. Scattering of the buffer was subtracted and the difference curves were scaled to unity protein concentration (1 mg/ml). Merging and further data analysis were carried out with version 2.8.4 of the ATSAS package [40]. The program CORAL [40] was used to compute theoretical SAXS curves based on the crystallographic homodimer, as well as to model missing loops and extremities. The SAXS data and corresponding CORAL model of the PptA dimer have been deposited in the SASBDB data base with accession number SASDF76.

Polyphosphate interaction

PolyP was obtained from (Sigma-Aldrich Chimie SARL, Saint-Quentin-Fallavier, France). To detect polyphosphatase activity, polyP was incubated with increasing amounts of PptA, in a buffer containing 20 mM Tris/HCl pH 7.4 and 200 mM NaCl. The effect of protein activity on polyP length was subsequently analysed using denaturing PAGE. An equal volume of denaturing sample buffer (89 mM Tris, 89 mM boric acid, 2 mM EDTA, 7M urea, 12% Ficoll) was added to the reactions, which were then applied to a gel containing 10% polyacrylamide (1 : 29), 89 mM Tris, 89 mM boric acid, 2 mM EDTA and 7M urea. The running buffer contained 89 mM Tris, 89 mM boric acid, 2 mM EDTA (1 × TBE). Electrophoresis at 15 V/cm was continued until the bromophenol blue that was loaded separately in a neighbouring lane had reached the bottom of the gel. PolyP was visualised using the negative staining method of Smith and Morrissey [41]. Similarly, physical interaction between polyP and PptA was analysed using an electrophoretic mobility shift assay (polyP-EMSA) based on native PAGE. The experimental set-up, buffers and gels were identical to those used for the polyphosphatase assays, except that urea was omitted from both gel and sample buffer.

Calorimetric experiments were carried out using a MicroCal PEAQ-ITC calorimeter (Malvern Pananalytical), according to the instructions provided by the manufacturer. All analyte samples contained 20 mM Tris/HCl pH 7.4 with 200 mM NaCl and were degassed immediately before use. The cell was loaded with 400 µL of a 100 µM PptA sample, whereas the syringe contained either 400 µM or 300 µM polyP with a chain length of 25 or 45 phosphates, respectively. Experiments were performed at 25 °C and involved successive 4 µL injections with 150 s intervals and a mixing speed of 500 Hz. Data were analysed using the MicroCal PEAQ-ITC software, assuming a single set of equivalent binding sites.

Results

Crystallographic analysis of PptA reveals a novel fold with unique structural features

For our structural studies, we chose a phosin from *Streptomyces chartreusis*. Compared to orthologs from

other streptomycetes, this protein contains fewer regions of low complexity that are likely to interfere with crystallisation. His_6-tagged PptA was expressed in *E. coli* and purified to homogeneity. Crystals were obtained that diffracted to 2.04 Å, allowing us to solve the structure by means of bromide SAD as described in Materials and methods.

As Fig. 1 shows, the PptA fold consists essentially of α-helices, pseudosymmetrically arranged to form a flat, lozenge-like structure. Arguably the most striking feature of the structure is a central tunnel, 5–10 Å in diameter that traverses the protein core. Its inner surface is highly positively charged as it is almost entirely made up of Arg side chains (Fig. 2). Three ordered sulfate ions, originating from the crystallisation buffer, are present within the confines of the tunnel and partially compensate its charge. The ions are contacted by a total of nine Arg residues, as well as a His and a Tyr side chain (Fig. 2B).

Intriguingly, two metal-binding sites could be identified in the structure. One of these is located in the interior of the protein, whereas the other lies on a crystallographic symmetry axis between adjacent molecules in the crystal lattice (Fig. 3). The presence of metal ions was initially deduced from unusually high-local electron densities (16 σ and 6.8 σ respectively) as well as the characteristic coordination of His side chains. Since it was not possible to establish the identity of the bound ions on the basis of our crystallographic data and the observed coordination chemistry alone [42], we analysed the metal content of PptA crystals by X-ray fluorescence (XRF) [37]. This experiment unambiguously revealed the presence of Cu^{2+}. In addition, a smaller signal corresponding to Zn^{2+} could be detected. Specific protein-metal ratios were determined by chemical means [38], revealing averages of 1.2 atoms of Cu^{2+} and 0.18 atoms of Zn^{2+} per protein molecule. Based on these results, we included the

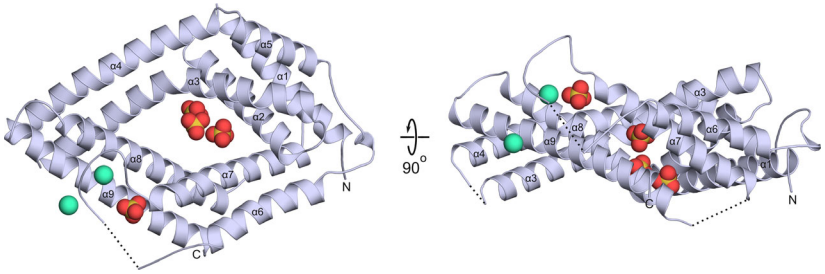

Fig. 1. The crystal structure of PptA, shown in two 90°-rotated views. Cu^{2+} ions are depicted in green, sulfates in yellow (sulfur) and red (oxygen). Dotted lines represent disordered loops for which no electron density was observed. Disordered regions at the N and C terminus are not shown.

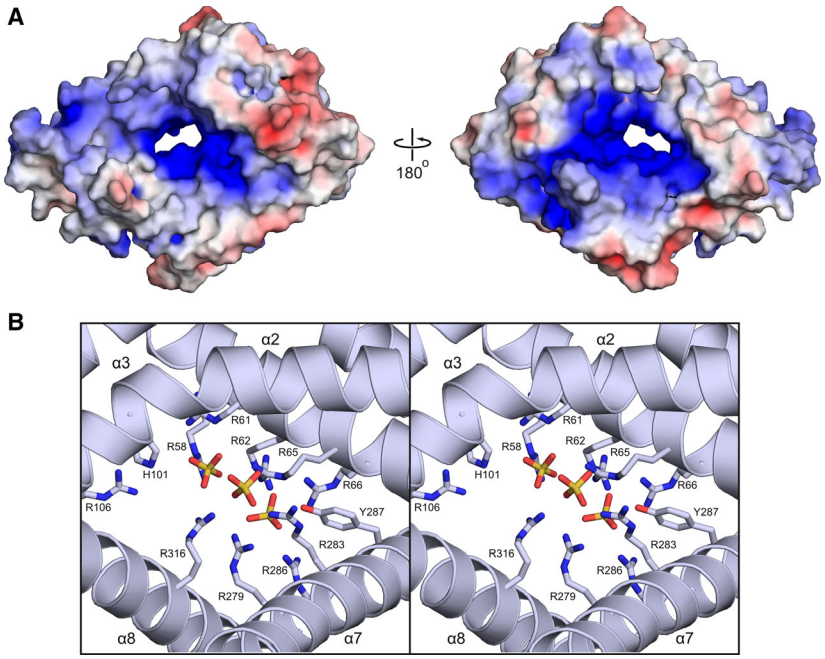

Fig. 2. PptA contains a positively charged tunnel traversing the protein core. (A) Surface charge distribution of PptA, represented by a colour spectrum from red (-5 kT/e) *via* white (0 kT/e) to blue (+5 kT/e). Panels correspond to 180°-rotated views. (B) Stereo view of the central tunnel and the Arg side chains lining it. Sulfate ions sequestered from the crystallisation buffer are shown. Also depicted are His and Tyr side chains that participate in sulfate binding.

FEBS Letters **593** (2019) 2019–2029 © 2019 The Authors. *FEBS Letters* published by John Wiley & Sons Ltd on behalf of Federation of European Biochemical Societies.

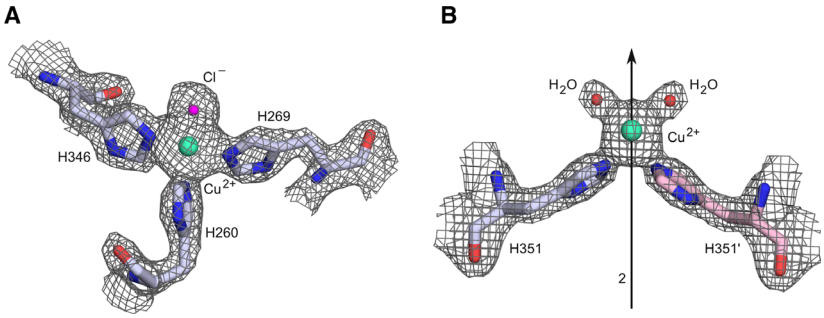

Fig. 3. The two metal-binding sites identified in PptA, with Cu^{2+} shown in green. (A) The intramolecular metal-binding site, with the final $2mF_o$-DF_c electron density map contoured at 2.0 σ. (B) The intermolecular metal-binding site, located on a crystallographic 2-fold symmetry axis (arrow). The $2mF_o$-DF_c electron density map shown here is contoured at 1.5 σ.

predominant metal ion, Cu^{2+}, in our final crystallographic model of PptA.

PptA forms stable homodimers in solution

The PISA analysis [43] of protein–protein contacts in the crystal suggested stable association of PptA into homodimers (Fig. 4A), with a buried interaction surface of 965 Å^2. The program predicted a ΔG^o of dissociation amounting to 6.5 kcal/mol, or 28.3 kcal/mol if metal ions were taken into account. In addition, gel filtration results, obtained using a Superdex 200 matrix (data not shown) pointed at a molecular mass of approximately 80 kDa, are consistent with dimer formation.

The oligomerisation state of PptA in solution was further investigated by small-angle X-ray scattering (SAXS), results of which are shown in Fig. 4B. Comparison of the Guinier-derived forward scattering (I_0) to that of a bovine serum albumin (BSA) reference indicated a particle mass of 58.8 kDa, whereas a recently developed concentration-independent Bayesian method [44] yielded a value of 78.5 kDa. These results are in good agreement with the expected mass of a

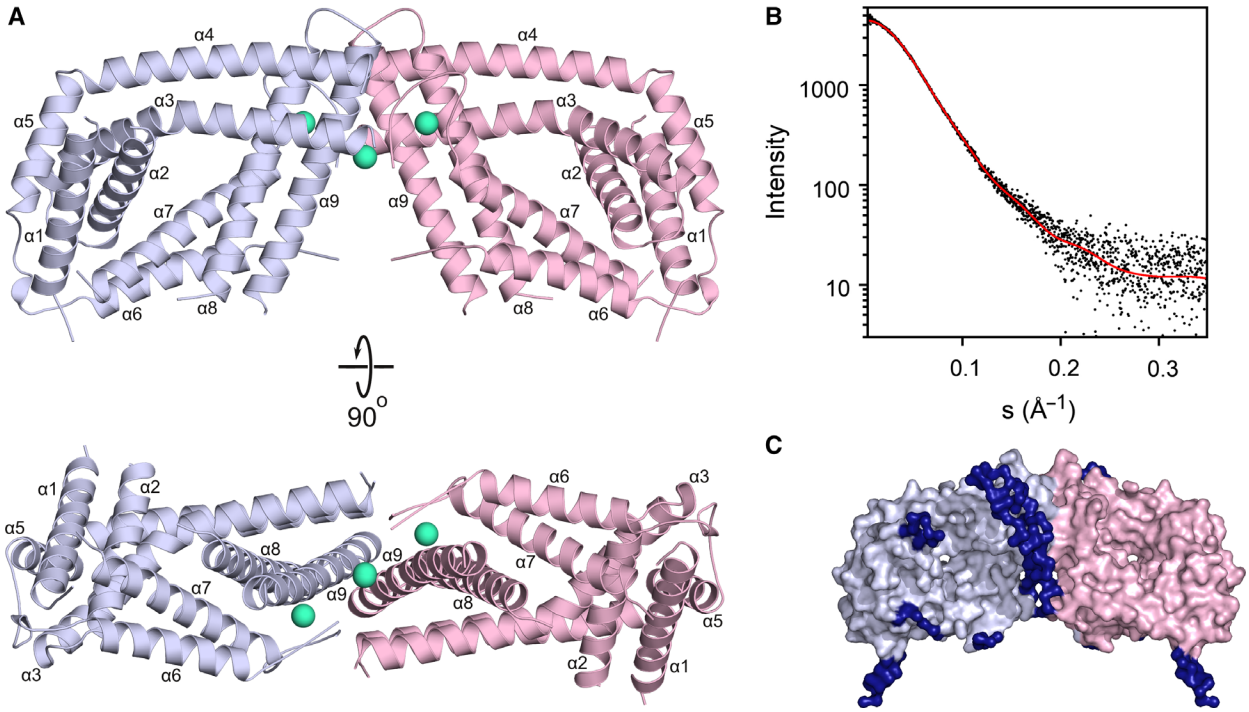

Fig. 4. PptA forms a stable dimer in solution. (A) The PptA dimer as observed in the crystal lattice, with subunits in blue and pink. The two images show 90°-rotated views. (B) Concentration-normalised scattering from a PptA solution (black dots). The momentum transfer is defined as $s = 4\pi \sin(\theta)/\lambda$, where 2θ is the scattering angle and $\lambda = 1.24$ Å is the X-ray wavelength. Theoretical scattering data for the dimer (red curve, $\chi^2 = 1.1$) were generated using the program CORAL [40], which accounted for loops that were missing in the crystallographic model. (C) Surface representation of the final model produced by CORAL, oriented as in the upper image of panel (A). Subunits of the dimer are shown in blue and pink, with regions added by CORAL in dark blue.

PptA dimer (79.2 kDa). A more detailed analysis was carried out with the program CORAL, which was used to add strings of dummy residues to the high-resolution crystallographic structure in order to account for missing loop regions as well as the undefined N- and C-terminal ends of the protein. The optimised model generated by CORAL (Fig. 4C) explains the experimental data to within experimental error (Fig. 4B, fitted curve in red), corroborating the dimerisation mode observed in the crystal lattice.

PptA binds with nanomolar affinity to polyphosphates

In view of the proximity of the *pptA* and *ppk* genes and their potential co-regulation, we hypothesised that the PptA protein might interact with polyP. The presence of a string of sulfate ions inside the tunnel also supports this idea, as occupation of phosphate-binding sites by sulfate is frequently observed in protein crystals obtained with sulfate as the main precipitant [45].

We first tested the hypothesis that PptA acts as a polyphosphatase, by analysing the stability of polyP in the presence and absence of the protein. However, the length of polyP molecules, reflected in their electrophoretic mobility under strongly denaturing conditions, was not affected by a 1 h preincubation with PptA (data not shown). We next asked whether PptA is able to stably interact with polyP. In contrast to results obtained under denaturing conditions, native PAGE of PptA-polyP mixtures (Fig. 5A) revealed a dramatic change in polyP electrophoretic mobility with increasing protein concentration, indicative of a direct and highly stable interaction. At low protein-polyP ratios, a complex characterised by a limited size and net negative charge migrated several millimetres below the top of the gel, as a single, discrete band. At higher protein-polyP ratios, as the available polyP started to become saturated, a low-mobility complex appeared that barely migrated into the gel at all. Presumably, the latter complex consisted of multiple PptA molecules bound to a single polyP chain, resulting in an increased overall size of the complex as well as a further reduction in its overall negative charge.

The interaction of PptA with polyP was analysed in more detail by means of isothermal calorimetry (ITC). Independent titrations with two polyP preparations of different chain length (Fig. 5B–D) produced similar results, indicating a K_d value around 100 nM and a binding site size of 14–15 phosphate moieties per PptA homodimer. Binding is entirely entropy-driven, with a positive ΔH^o and a strongly negative -TΔS^o contribution to ΔG^o, the standard free energy change (Fig. 5D).

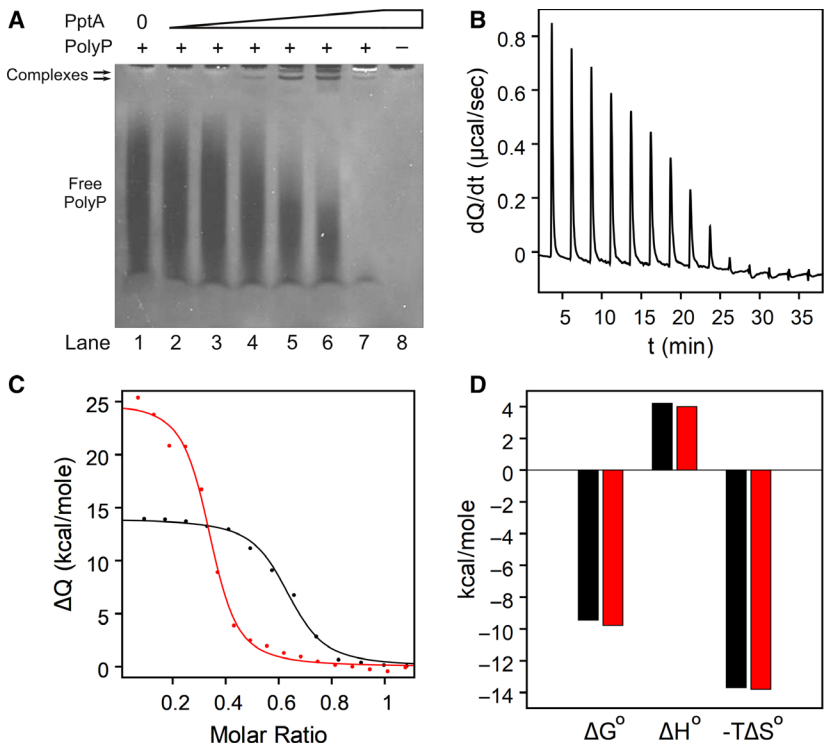

Fig. 5. Interaction of PptA with polyP. (A) PolyP electrophoretic mobility shift assay (polyP-EMSA). (B) Raw ITC data for 25-mer polyP. (C) Fitted binding curves for 25-mer (black) and 45-mer (red) polyP. The molar ratio is defined as the polyP concentration divided by the PptA dimer concentration. (D) Summary of the thermodynamic characteristics of the interaction, determined using 25-mer and 45-mer polyP (colours as in C). According to these independent analyses, a single PptA dimer binds 15.0 and 14.4 phosphate units respectively.

FEBS Letters **593** (2019) 2019–2029 © 2019 The Authors. *FEBS Letters* published by John Wiley & Sons Ltd on behalf of Federation of European Biochemical Societies.

Discussion

In the study presented here, we analysed the structural and biochemical properties of a phosin (PptA) from *S. chartreusis*. The highly unusual polyphosphate- and metal-binding fold that we identify has not been described in the literature, but bears similarity to a previously deposited crystal structure (PDB entry 3E0S). The latter, annotated as an uncharacterised protein from *Chlorobaculum tepidum*, was solved in the context of a structural genomics initiative. Superposition of the two structures *via* secondary structure matching in the program Coot [31,32] yields a C_α-RMSD of 2.9 Å for a total of 244 aligned residues (Fig. 6). Like PptA of *S. chartreusis*, 3E0S consists entirely of α-helices that together form a thin, pseudosymmetrical lozenge with a central tunnel running through its core. As the superposition shows, the relative positioning of most α-helices varies considerably between the two structures, as does their length. Moreover, several α-helices are missing in PptA. In spite of these marked differences and the very limited sequence identity between the two proteins (14.5% in the structure-based alignment shown in Fig. 6B, excluding gaps), the net positive charge of the tunnel surface is essentially conserved. Similar to PptA, 3E0S features

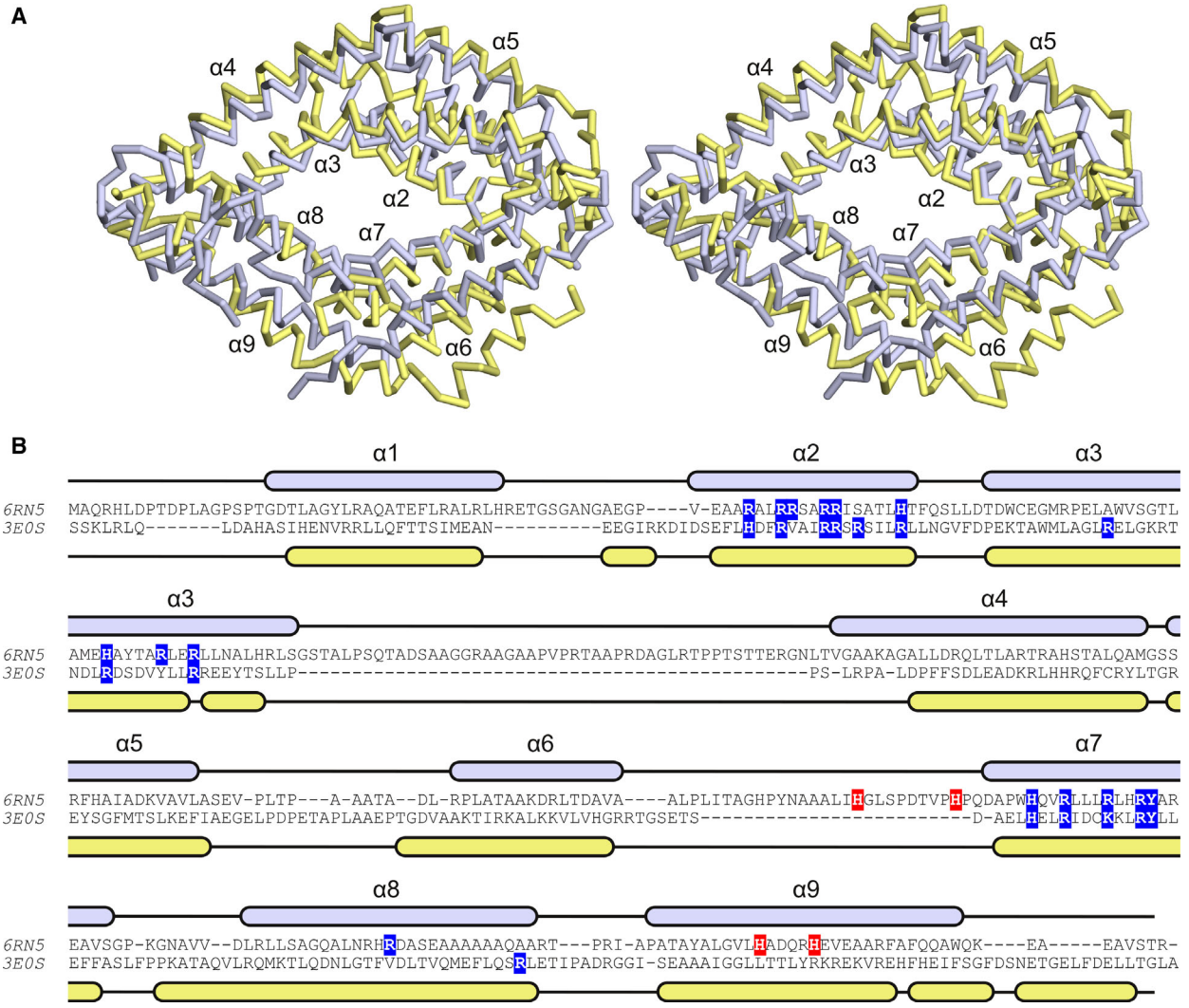

Fig. 6. Comparison of the PptA structure solved in the present study (6RN5, blue) and PDB entry 3E0S, PptB from *Clorobium tepidum* (yellow). (A) Stereo image of the superposed structures, shown as C_α traces. (B) Structure-based alignment of the protein sequences. Metal-binding His residues are shown in red, whereas sulfate-binding and positively charged residues lining the tunnel surface are shown in blue.

multiple sulfate ions apparently sequestered from the crystallisation buffer. These observations strongly suggest that 3E0S and other divergent members of the CHAD family are also capable of polyP binding. Dimerisation appears to be conserved, as a very similar 2-fold symmetrical arrangement is present in the 3E0S crystal lattice. The two homodimeric assemblies can be superimposed with a C_α-RMSD of 4.2 Å for a total of 490 aligned residues. In contrast, the two metal-binding sites that we identified in PptA have no direct counterparts in 3E0S, perhaps reflecting the existence of multiple CHAD families that differ in their metal-binding ability or specificity. Like other phosins, 3E0S is rich in His residues that may constitute alternative binding sites, while the absence of metal ions in the experimentally determined structure could be a consequence of the protein purification or crystallisation procedure.

The biological consequences of polyP binding by phosins remain unknown. PolyP is an ancient and ubiquitous biological polymer, thought to act as a reserve of both phosphate and energy during nutritional stress [46,47]. In addition, a role in signalling has been proposed [48]. Earlier work has revealed that Ppk, the bacterial kinase responsible for polyP synthesis and the regeneration of ATP from ADP and polyP, plays a negative role in the regulation of antibiotic production by *Streptomyces lividans* in conditions of phosphate limitation [22–24]. The fact that in streptomycetes PptA is encoded by a gene immediately downstream of *ppk* may point at related functions of the proteins in phosphate metabolism and, conceivably, in the regulation of antibiotic synthesis. Interestingly, recent microscopic studies revealed a striking co-localisation of PptA and polyP granules in several prokaryotes [26]. The direct, high-affinity interaction between PptA and polyP that we describe in the present study readily explains these findings. In earlier studies, Ppk co-localised in similar fashion with polyP granules [49,50], consistent with the idea that the two proteins act in concert. One attractive possibility is that PptA assists Ppk in the mobilisation of polyP reserves at the onset of P_i limitation. Intriguingly, the gene immediately downstream of *ppk* in *E. coli* and most other bacteria does not encode PptA but a polyphosphatase, Ppx. However, we failed to detect any polyphosphatase activity in PptA. This could indicate that PptA acts as a cofactor or processivity factor, either to Ppk or to a true polyphosphatase. PptA forms stable dimers in solution, which implies that the protein could, in principle, bind two strands of polyP simultaneously and thereby physically link the polymer chains in a non-covalent manner. A critical role of such a mechanism in the nucleation or growth of aggregates seems unlikely, given that polyP granules were also found in PptA knock-out mutants [26]. However, this observation does not rule out a qualitative impact of PptA binding on granule structure. PptA might, for instance, render polyP molecules at the surface of granules more accessible to Ppk or polyphosphatases.

Our observation that a phosin from *S. chartreusis* binds Cu^{2+} is intriguing, as this particular metal ion is seldom found in bacterial cytoplasmic proteins. In most cases, the metal either acts as a cofactor in enzymes or is sequestered by specialised proteins responsible for its storage and detoxification. In *Streptomyces*, considerable variations in the cytoplasmic Cu^{2+} concentration accompany development [51] and strongly influence germination, differentiation and antibiotic synthesis [51–54]. Consistent with these key regulatory roles, Cu^{2+} levels are precisely controlled [51] by means of a dedicated import and export machinery that includes a recently discovered chalkophore [55]. It is conceivable that PptA acts as a sensor or modifier of the intracellular Cu^{2+} concentration, while simultaneously measuring or affecting polyphosphate availability. Thus, the protein might mediate cross-talk between two critical nutrient-sensing pathways, both of which have been linked to morphological development and antibiotic production. It is also possible that PptA is involved in stripping divalent metal ions from polyP, which is itself a strong chelator with known roles in metal storage [46]. Such an activity might not only serve to increase free metal ion concentrations in the cytosol, but also to bring polyP into an extended form that may be more readily metabolised. Further studies will be required to investigate the effects of the interaction of PptA with metals and polyP *in vivo*, as well as to establish if the protein influences development and antibiotic production in *Streptomyces*.

Acknowledgements

Beamline staff of BESSY and the EMBL outstation at DESY are gratefully acknowledged for their kind assistance during data collection.

Author contributions

SW conceived and supervised this study; SW, NHR and MG performed experiments and analysed data; MJV and WH provided reagents, facilities and helpful advice; SW wrote the manuscript and made revisions.

References

1 Challis GL and Hopwood DA (2003) Synergy and contingency as driving forces for the evolution of

multiple secondary metabolite production by *Streptomyces* species. *Proc Natl Acad Sci USA* **100**, 14555–14561.
2 Hopwood DA (2007) *Streptomyces* in Nature and Medicine: the Antibiotic Makers. Oxford University Press, New York, NY.
3 Watve MG, Tickoo R, Jog MM and Bhole BD (2001) How many antibiotics are produced by the genus *Streptomyces*? *Arch Microbiol* **176**, 386–390.
4 Baltz RH (2008) Renaissance in antibacterial discovery from actinomycetes. *Curr Opin Pharmacol* **8**, 557–563.
5 Genilloud O (2017) Actinomycetes: still a source of novel antibiotics. *Nat Prod Rep* **34**, 1203–1232.
6 Hug JJ, Bader CD, Remškar M, Cirnski K and Müller R (2018) Concepts and methods to access novel antibiotics from actinomycetes. *Antibiotics (Basel)* **7**, E44.
7 Martín JF, Liras P and Demain AL (1978) ATP and adenylate energy charge during phosphate-mediated control of antibiotic synthesis. *Biochem Biophys Res Commun* **83**, 822–828.
8 Lounès A, Lebrihi A, Benslimane C, Lefebvre G and Germain P (1996) Regulation of spiramycin synthesis in *Streptomyces ambofaciens*: effects of glucose and inorganic phosphate. *Appl Microbiol Biotechnol* **45**, 204–211.
9 Martín JF (2004) Phosphate control of the biosynthesis of antibiotics and other secondary metabolites is mediated by the PhoR-PhoP system: an unfinished story. *J Bacteriol* **186**, 5197–5201.
10 Rodríguez-García A, Barreiro C, Santos-Beneit F, Sola-Landa A and Martín JF (2007) Genome-wide transcriptomic and proteomic analysis of the primary response to phosphate limitation in *Streptomyces coelicolor* M145 and in a ΔphoP mutant. *Proteomics* **7**, 2410–2429.
11 Sola-Landa A, Moura RS and Martín JF (2003) The two-component PhoR-PhoP system controls both primary metabolism and secondary metabolite biosynthesis in *Streptomyces lividans*. *Proc Natl Acad Sci USA* **100**, 6133–6138.
12 Hsieh YJ and Wanner BL (2010) Global regulation by the seven-component Pi signaling system. *Curr Opin Microbiol* **13**, 198–203.
13 Sola-Landa A, Rodríguez-García A, Franco-Domínguez E and Martín JF (2005) Binding of PhoP to promoters of phosphate-regulated genes in *Streptomyces coelicolor*: identification of PHO boxes. *Mol Microbiol* **56**, 1373–1385.
14 Rodríguez-García A, Sola-Landa A, Apel K, Santos-Beneit F and Martín JF (2009) Phosphate control over nitrogen metabolism in *Streptomyces coelicolor*: direct and indirect negative control of glnR, glnA, glnII and amtB expression by the response regulator PhoP. *Nucleic Acids Res* **37**, 3230–3242.
15 Allenby NE, Laing E, Bucca G, Kierzek AM and Smith CP (2012) Diverse control of metabolism and other cellular processes in *Streptomyces coelicolor* by the PhoP transcription factor: genome-wide identification of in vivo targets. *Nucleic Acids Res* **40**, 9543–9556.
16 Smirnov A, Esnault C, Prigent M, Holland IB and Virolle MJ (2015) Phosphate homeostasis in conditions of phosphate proficiency and limitation in the wild type and the phoP mutant of *Streptomyces lividans*. *PLoS ONE* **10**, e0126221.
17 Apel AK, Sola-Landa A, Rodríguez-García A and Martín JF (2007) Phosphate control of phoA, phoC and phoD gene expression in *Streptomyces coelicolor* reveals significant differences in binding of PhoP to their promoter regions. *Microbiology* **153**, 3527–3537.
18 Santos-Beneit F, Rodríguez-García A, Apel AK and Martín JF (2009) Phosphate and carbon source regulation of two PhoP-dependent glycerophosphodiester phosphodiesterase genes of *Streptomyces coelicolor*. *Microbiology* **155**, 1800–1811.
19 Díaz M, Esteban A, Fernández-Abalos JM and Santamaría RI (2005) The high-affinity phosphate-binding protein PstS is accumulated under high fructose concentrations and mutation of the corresponding gene affects differentiation in *Streptomyces lividans*. *Microbiology* **151**, 2583–2592.
20 Santos-Beneit F, Rodríguez-García A, Franco-Domínguez E and Martín JF (2008) Phosphate-dependent regulation of the low- and high-affinity transport systems in the model actinomycete *Streptomyces coelicolor*. *Microbiology* **154**, 2356–2370.
21 Ghorbel S, Smirnov A, Chouayekh H, Sperandio B, Esnault C, Kormanec J and Virolle MJ (2006) Regulation of ppk expression and in vivo function of Ppk in *Streptomyces lividans* TK24. *J Bacteriol* **188**, 6269–6276.
22 Chouayekh H and Virolle MJ (2002) The polyphosphate kinase plays a negative role in the control of antibiotic production in *Streptomyces lividans*. *Mol Microbiol* **43**, 919–930.
23 Esnault C, Dulermo T, Smirnov A, Askora A, David M, Deniset-Besseau A, Holland IB and Virolle MJ (2017) Strong antibiotic production is correlated with highly active oxidative metabolism in *Streptomyces coelicolor* M145. *Sci Rep* **7**, 200.
24 Le Maréchal P, Decottignies P, Marchand CH, Degrouard J, Jaillard D, Dulermo T, Froissard M, Smirnov A, Chapuis V and Virolle MJ (2013) Comparative proteomic analysis of *Streptomyces lividans* wild-type and ppk mutant strains reveals the importance of storage lipids for antibiotic biosynthesis. *Appl Environ Microbiol* **79**, 5907–5917.
25 Iyer LM and Aravind L (2002) The catalytic domains of thiamine triphosphatase and CyaB-like adenylyl

cyclase define a novel superfamily of domains that bind organic phosphates. *BMC Genom* **3**, 33.
26 Tumlirsch T and Jendrossek D (2017) Proteins with CHADs (Conserved Histidine α-Helical Domains) are attached to polyphosphate granules in vivo and constitute a novel family of polyphosphate-associated proteins (Phosins). *Appl Environ Microbiol* **83**, e03399–16.
27 Mueller U, Darowski N, Fuchs MR, Frster R, Hellmig M, Paithankar KS, Phringer S, Steffien M, Zocher G and Weiss MS (2012) Facilities for macromolecular crystallography at the Helmholtz-Zentrum Berlin. *J Synch Rad* **19**, 442–449.
28 Kabsch W (2010) XDS. *Acta Crystallogr D Biol Crystallogr* **66**, 125–132.
29 McCoy AJ, Grosse-Kunstleve RW, Adams PD, Winn MD, Storoni LC and Read RJ (2007) Phaser crystallographic software. *J Appl Crystallogr* **40**, 658–674.
30 Adams PD, Afonine PV, Bunkóczi G, Chen VB, Davis IW, Echols N, Headd JJ, Hung LW, Kapral GJ, Grosse-Kunstleve RW *et al.* (2010) PHENIX: a comprehensive python-based system for macromolecular structure solution. *Acta Crystallogr D Biol Crystallogr* **66**, 213–221.
31 Emsley P and Cowtan K (2004) Coot: Model-building tools for molecular graphics. *Acta Crystallogr D Biol Crystallogr* **60**, 2126–2132.
32 Emsley P, Lohkamp B, Scott WG and Cowtan K (2010) Features and development of Coot. *Acta Crystallogr D Biol Crystallogr* **66**, 486–501.
33 Murshudov GN, Vagin AA and Dodson EJ (1997) Refinement of macromolecular structures by the maximum-likelihood method. *Acta Crystallogr D Biol Crystal-logr* **53**, 240–255.
34 Murshudov GN, Skubák P, Lebedev AA, Pannu NS, Steiner RA, Nicholls RA, Winn MD, Long F and Vagin AA (2011) REFMAC5 for the refinement of macromolecular crystal structures. *Acta Crystallogr D Biol Crystallogr* **67**, 355–367.
35 Programs for Protein Crystallography (1994) Collaborative computational project, number 4. The CCP4 suite. *Acta Crystallogr D Biol Crystallogr* **50**, 760–763.
36 Baker NA, Sept D, Joseph S, Holst MJ and McCammon JA (2001) Electrostatics of nanosystems: application to microtubules and the ribosome. *Proc Natl Acad Sci USA* **98**, 10037–10041.
37 Hagedoorn PL (2015) Microbial metalloproteomics. *Proteomes* **3**, 424–439.
38 Säbel CE, Neureuther JM & Siemann S (2010) A spectrophotometric method for the determination of zinc, copper, and cobalt ions in metalloproteins using zincon. *Anal Biochem* **397**, 218–226.
39 Blanchet CE, Spilotros A, Schwemmer F, Graewert MA, Kikhney AG, Jeffries CM, Franke D, Mark D, Zengerle R, Cipriani F *et al.* (2015) Versatile sample environments and automation for biological solution X-ray scattering experiments at the P12 beamline (PETRA III, DESY). *J Appl Cryst* **48**, 431–443.
40 Petoukhov MV, Franke D, Shkumatov AV, Tria G, Kikhney AG, Gajda M, Gorba C, Mertens HDT, Konarev PV and Svergun DI (2012) New developments in the ATSAS program package for small-angle scattering data analysis. *J Appl Cryst* **45**, 342–350.
41 Smith SA and Morrissey JH (2007) Sensitive fluorescence detection of polyphosphate in polyacrylamide gels using 40,6-diamidino-2-phenylindol. *Electrophoresis* **28**, 3461–3465.
42 Zheng H, Chruszcz M, Lasota P, Lebioda L and Minor W (2008) Data mining of metal ion environments present in protein structures. *J Inorg Biochem* **102**, 1765–1776.
43 Krissinel E and Henrick K (2007) Inference of macromolecular assemblies from crystalline state. *J Mol Biol* **372**, 774–797.
44 Hajizadeh NR, Franke D, Jeffries CM and Svergun DI (2018) Consensus Bayesian assessment of protein molecular mass from solution X-ray scattering data. *Sci Rep* **8**, 7204.
45 Copley RR and Barton GJ (1994) A structural analysis of phosphate and sulphate binding sites in proteins. Estimation of propensities for binding and conservation of phosphate binding sites. *J Mol Biol* **242**, 321–329.
46 Kornberg A, Rao NN and Ault-Riché D (1999) Inorganic polyphosphate: a molecule of many functions. *Annu Rev Biochem* **68**, 89–125.
47 Brown MR and Kornberg A (2008) The long and short of it | polyphosphate, PPK and bacterial survival. *Trends Biochem Sci* **33**, 284–290.
48 Rao NN and Kornberg A (1999) Inorganic polyphosphate regulates responses of *Escherichia coli* to nutritional stringencies, environmental stresses and survival in the stationary phase. *Prog Mol Subcell Biol* **23**, 183–195.
49 Henry JT and Crosson S (2013) Chromosome replication and segregation govern the biogenesis and inheritance of inorganic polyphosphate granules. *Mol Biol Cell* **24**, 3177–3186.
50 Tumlirsch T, Sznajder A and Jendrossek D (2015) Formation of polyphosphate by polyphosphate kinases and its relationship to poly(3-Hydroxybutyrate) accumulation in Ralstonia eutropha strain H16. *Appl Environ Microbiol* **81**, 8277–8293.
51 González-Quiñónez N, Corte-Rodríguez M, Álvarez-Fernández-García R, Rioseras B, López-García MT, Fernández-García G, Montes-Bayón M, Manteca A and Yagüe P (2019) Cytosolic copper is a major

modulator of germination, development and secondary metabolism in *Streptomyces coelicolor*. *Sci Rep* **9**, 4214.

52 Ueda K, Tomaru Y, Endoh K and Beppu T (1997) Stimulatory effect of copper on antibiotic production and morphological differentiation in *Streptomyces tanashiensis*. *J Antibiot (Tokyo)* **50**, 693–695.

53 Keijser BJ, van Wezel GP, Canters GW, Kieser T and Vijgenboom E (2000) The Ram-dependence of *Streptomyces lividans* differentiation is bypassed by copper. *J Mol Microbiol Biotechnol* **2**, 565–574.

54 Worrall JA and Vijgenboom E (2010) Copper mining in *Streptomyces*: enzymes, natural products and development. *Nat Prod Rep* **27**, 742–756.

55 Wang L, Zhu M, Zhang Q, Zhang X, Yang P, Liu Z, Deng Y, Zhu Y, Huang X, Han L *et al*. (2017) Diisonitrile natural product SF2768 functions as a Chalkophore that mediates copper acquisition in *Streptomyces thioluteus*. *ACS Chem Biol* **12**, 3067–3075.